Journal of Materials Chemistry C

ROYAL SOCIETY OF CHEMISTRY

PAPER

View Article Online
View Journal | View Issue

Cite this: J. Mater. Chem. C, 2024, 12, 3228

Investigation and control of metallogel formation for the deposition of supramolecular nanotubes of single-chain magnets†

Felix Houard, [a] Andrea Olivier,[a] Giuseppe Cucinotta, [b] Olivier Galangau, [a] Marie Gautier,[d] Franck Camerel,[a] Thierry Guizouarn,[a] Thierry Roisnel, [a] Boris Le Guennic, [a] Mykhaylo Ozerov, [c] Yan Suffren, [a] Guillaume Calvez, [a] Carole Daiguebonne,[a] Olivier Guillou, [a] Franck Artzner,[d] Matteo Mannini *[b] and Kevin Bernot *[ae]

Received 6th October 2023,
Accepted 26th January 2024

DOI: 10.1039/d3tc03630h

rsc.li/materials-c

Metallogels are versatile and intriguing objects that can be used as media for the deposition of extended molecular architectures on surfaces. In this work, we investigate the thermodynamic and kinetics conditions that induce robust metallogel formation from supramolecular nanotubes of single-chain magnets (SCM). These latter are made of woven chains that alternate Tb and nitronyl-nitroxide radical building blocks. By tailoring the size of the alkyl chain grafted on the radical (**NITPhOCn**, with n = 6, 10, or 18) we show that long alkyl chains induce delicate gelation conditions but provide gels with improved stability against crystallization and enhanced deposition ability while preserving the overall SCM behaviour of the molecular nanotubes.

Introduction

Magnetic materials play a prominent role in our modern society, finding essential applications in numerous industrial sectors (electric power generation, transportation, electronics, and communications) as well as in our daily lives.[1] One such area of application is digital data storage,[2] where the demand for increased storage capacity continues to grow exponentially.[3]

To address this challenge, collaborative efforts between chemists and physicists have led to the development of superparamagnetic molecules known as Single-Molecule Magnets (SMMs),[4–7] where the magnetic anisotropy of the 3d or 4f metal ions is judiciously enhanced by surrounding organic ligands.[8–12] These discrete molecules exhibit a sufficiently slow relaxation of their magnetization, allowing them to act as individual bits at the molecular scale and making them promising candidates for high-density data storage.[13–15]

The nanometric dimensions of SMMs also enable quantum properties such as quantum tunnelling of the magnetization (QTM).[16] This latter has been envisioned as crucial for SMM exploitation in quantum computing and spintronics,[17–21] but is highly detrimental for molecular magnetic data storage. Additionally, the precise design of such molecules limits the balance between the improvement of the blocking temperature T_B, the maximum temperature for which an open magnetic hysteresis is observed, and their chemical integrity toward external factors (temperature, air, moisture, interaction with a substrate, *etc.*).

These limitations can be overcome by increasing the dimensionality of the molecular magnet to obtain one-dimensional analogues called Single-Chain Magnets (SCMs), made of anisotropic magnetic centres that alternate to form infinite coordination polymers.[22–24] Intrachain exchange interactions induce the rise of spin correlation phenomena at low temperature along the chain, whose relaxations obey Glauber dynamics, less impacted by QTM and other SMM's relaxation processes.[25,26] An efficient strategy to synthesize SCMs is to use bidentate nitronyl nitroxide radicals (NIT)[27] as linkers between the anisotropic magnetic 4f ions.[28,29] Then, their functionalization allows tuning their structural and magnetic properties.[30–32]

Following this approach, our groups have recently reported the synthesis of a nitronyl-nitroxide radical functionalized with a hexyloxy- pendant chain, here named **NITPhOC6**

[a] Univ Rennes, INSA Rennes, CNRS, ISCR (Institut des Sciences Chimiques de Rennes), UMR, Université de Rennes, 6226, Rennes, France. E-mail: kevin.bernot@insa-rennes.fr
[b] Dipartimento di Chimica "Ugo Schiff" (DICUS), Università degli Studi di Firenze, INSTM Research Unit of Firenze, Sesto Fiorentino, Italy
[c] National High Magnetic Field Laboratory, Florida State University, Tallahassee, FL, 32310, USA
[d] CNRS, IPR (Institut de Physique de Rennes), UMR, Université de Rennes, 6251, Rennes, France
[e] Institut Universitaire de France, Paris, France

† Electronic supplementary information (ESI) available. CCDC 2298965–2298968. For ESI and crystallographic data in CIF or other electronic format see DOI: https://doi.org/10.1039/d3tc03630h

(2-(4′-hexoxyphenyl)-4,4,5,5-tetramethyl-imidazolin-1-oxyl-3-oxide). Its coordination with $Tb(hfac)_3$ units ($hfac^-$ = hexafluoroacetylacetonate) led to the crystallization of chiral nanotubes favoured by supramolecular interactions between the constituting helical chains, while featuring targeted SCM behaviour including memory effect of molecular origin.[33] However, despite this unusual nanotubular arrangement, deposition on the surface of such crystalline SCMs remained unfruitful, making it physically impossible to study their magnetic behaviour on surfaces for data storage purposes.

Indeed, nanostructuration is the necessary step towards the technological use of these molecules.[13,14] To date, the deposition of SMMs on surfaces has been more extensively studied than that of SCMs, due to their simpler structure, which allows us to control, to some extent, the difficulties associated with nanostructuration. These difficulties are mainly associated with preserving the chemical integrity of these molecules against external factors (temperature, presence of specific competing chemical agents such as water, pressure variations, or more importantly interactions with the substrate).

To overcome these processability limitations, a promising approach is to stabilize these polymeric chains in the form of metallogels, easier to shape and process,[34] while preserving their targeted responsive properties.[35–38] In particular, some groups have taken advantage of this strategy by designing ligands with long lipophilic alkyl chains, in order to promote the gelation of polymeric Fe^{II} triazolate chains exhibiting spin-crossover effects.[39,40]

In our case, by increasing the size of the alkyl chain beard by the NIT ligand up to 18 carbon atoms (**NITPhOC18**, (2-(4′-octadecyloxyphenyl)-4,4,5,5-tetramethylimidazolin-1-oxyl-3-oxide)), we have successfully stabilized these nanotubular SCMs in a metallogel phase while preserving their magnetic properties.[41] Taking advantage of the improved processability of the metallogels, isolated nanotubes of SCMs were observed on the surface by AFM.

The influence of the variation of pendant alkyl tail length on the self-assembly process of supramolecular systems is known to provide different morphologies[42–44] or physicochemical properties.[45–47] This is the reason why we focused on this aspect by studying a series of SCMs later called **TbCn** (where n = 6, 10, or 18, the number of carbon atoms constituting the alkyl chain used to functionalize the nitronyl nitroxide group). The detailed physicochemical parameters that govern the self-assembly process of the supramolecular nanotubes, the corresponding metallogels formation, and their stability have been explored in order to rationalize the formation of metallogels of supramolecular nanotubes of SCMs.

Results and discussion

Synthetic procedure and gelation properties

To evaluate the impact of the carbon tail length on the gelation properties as well as on the stability of the SCM, a comparative study was held with NIT radical derivatives, **NITPhOCn**, bearing aliphatic chains of different length (n = 6, 10, or 18), have been synthesized following the standard Ullman procedure[48] and obtained as dark-blue powders (see Fig. S1, ESI†).

Following the protocol reported in our previous study,[41] their coordination with one equivalent of $Tb(hfac)_3$ complex in hot n-heptane affords dark green amorphous powders (see Fig. 1 and Fig. S3, ESI†) once the solvent was removed. They are used as starting materials for the gelation and are later called **Pre-TbCn** (with n = 6, 10, or 18).

The chemical purity of the powders was probed using FTIR, EA, and luminescence measurements (Fig. S4 and S5, ESI†). The sensitivity of the photoluminescence was exploited to probe the presence of uncoordinated reactants, especially the $Tb(hfac)_3{\cdot}2H_2O$, which shows well-defined line-shaped bands close to the ones of the free Tb^{III} ion. Hence, the observation of such emission bands at 487, 542, 583, 617, and 650 nm in the luminescent spectra of the solid indicates that a fraction of uncoordinated Tb reactant was still present in noticeable proportions for the **Pre-TbC6**, and in a less extend for the **Pre-TbC10** and **Pre-TbC18** ones (see Fig. S5, ESI†).

To tackle the presence of impurities, an ultrasonication step was introduced before solvent removal, by delivering around E = 85 kJ over one hour by pulsed sonication (see detailed method in ESI†). As demonstrated previously by our group,[49] this approach is relevant for preventing the presence of unreacted $Tb(hfac)_3$ particles by promoting a more effective reaction between the building blocks. Hence, the comparison between the non-sonicated (or ''conventional'') and ultrasonicated emission spectra showed a substantial decrease in the main Tb^{III} band intensities (Fig. S5, ESI†), attesting to an improved purity.

As previously observed for the **TbC18** gel, only aliphatic solvents allow effective gelation of **TbCn** compounds (Table S2, ESI†). The other solvents compete with the formation of coordinate bonds by excessive solubilization/solvation of the building blocks, thus hindering the formation of a π-stacking assembly between the aromatic $hfac^-$ and NIT phenyl moieties.[50–52] After a few minutes of cooling at 4 °C, the dark blue hot solutions turned into translucent cyan **TbCn** gels which did not flow once the vial was inverted.

Liquid-gel pseudo-phase diagrams were determined for different mass concentrations (C_M) *via* the test tube inversion method for different temperatures, upon cooling of hot *n*-heptane solutions of **Pre-TbCn** (see Instrument and methods in ESI†). One can note that a quenching step at a rate of $\Delta T/\Delta t$ = 10 °C min^{-1} is mandatory to obtain the gel phases in a reproducible way. This is characteristic of a kinetic gelling process, while a slower cooling (1 or 0.1 °C min^{-1}) leads to a mixture of liquid and unstable gels that hinder the precise determination of the gelling temperature. To characterize these pseudo-phase transitions, Dynamic Scanning Calorimetry (DSC) measurements have been performed on the *n*-heptane gels in sealed pan at different concentrations (C_M = 10 and 50 mg mL^{-1}) and thermal scan rates ($\Delta T/dt$ = 10, 1 and 0.1 K s^{-1}). Under these conditions, no endo- or exothermic peaks could be observed (Fig. S6–S8, ESI†) that confirms that a progressive

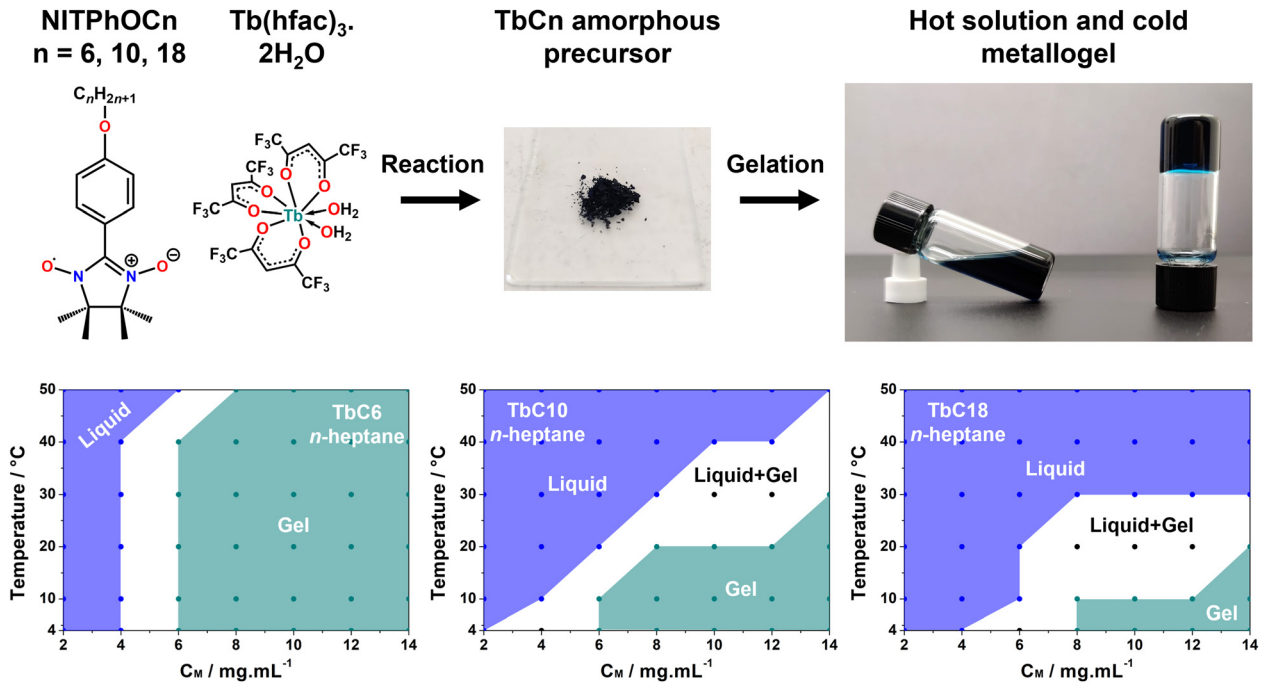

Fig. 1 Schematic procedure for the synthesis of the **TbCn** metallogels (top). Liquid/gel pseudo-phase diagrams of fresh *n*-heptane kinetic gels of **TbC6**, **TbC10** and **TbC18** (bottom).

aggregation process involving weak intermolecular interactions is at the origin of the gelation. Nevertheless, we have also determined the melting temperatures of **TbCn** *n*-heptane gels by the inverted test tube technique, 36, 37 and 40 ± 1 °C for **TbC6**, **TbC10** and **TbC18** gels respectively.

Last, liquid-gel pseudo-phase diagram of **TbC6** shows a gel region over a wide range of C_M concentrations and temperatures (50–4 °C). This indicates the occurrence of an efficient self-assembling as well as of the gelation process, even for a quite short alkyl chain. Then, when comparing with **TbC10** and **TbC18**, the bigger the alkyl chain, the smaller the gel domain is. This somewhat counterintuitive observation at first sight, could be related to the solubility trend of the radical in *n*-heptane (the longer the more soluble). This finding is also balanced by the gel stability toward crystallization that goes from some hours for **TbC6**, to days for **TbC10** and even months for **TbC18** (see also SAXS investigations below), that confirms the metastable nature of the gels.

Rheological measurements were conducted on the **TbC10** (Fig. 3) and **TbC18** gels (Fig. S9, ESI†), the **TbC6** being too fragile and break when transferred on the rheometer stage. The storage G' modulus exceed G'' with strain less than 10% for **TbC10** and less than 25% for **TbC18**. This unambiguously demonstrates a characteristic viscoelastic behaviour, and the gel nature of the samples.

Spectroscopic studies of the gelation process

From these macroscopic observations, it sounds clear that kinetics strongly influences the gelation. To gain insights into this process, UV-visible spectroscopy measurements as a function of time were carried out for the three *n*-heptane sol–gel systems of **TbCn** (Fig. 2a–c) at a fixed mass concentration (C_M = 10 mg mL^{-1}).

Prior to the measurement, all the **TbCn** solutions were thermalized and homogenized at 50 °C, with a characteristic blue colour. Then, UV-visible absorption was monitored upon rapid cooling (10 °C min^{-1}) to reach characteristic green gels at 4 °C for all derivatives, in agreement with the liquid-gel pseudo-phase diagrams (Fig. 1). All spectra show the characteristic four peaks observed on compounds made of lanthanide and aromatic nitronyl-nitroxide derivatives[53] that are associated to the transitions of the radical (Fig. S10, ESI†).[54]

Then, as the temperature decreases the most obvious feature is an increase of absorbance associated with a bathochromic shift (from approximately 625 to 645 nm) of the main absorption band of the radical. The peak increases quickly during the first minutes of sol–gel transformation with a quasi-linear evolution, that could be associated with the coordination between **NITPhOCn** and Tb(hfac)$_3$ moieties. It is also stressed by the presence of isosbestic points around 485 and 600 nm, which reflect the balance between the NIT ligands and Tb^{III} complexes, and the progressive appearance of mono/oligomers of **TbCn** in solution. After 5 minutes, a plateau is reached concomitantly with the temperature stabilization at 4 °C (Fig. 2d). Notably, the coordination kinetics seems to be slightly faster for **TbC6**, possibly because of the smaller steric hindrance of its alkyl chain compare to **TbC10** and **TbC18**.

Then, several shoulders evolve during the formation of the gel phases at 4 °C. Upon cooling, the first shoulder at 575 nm is smoothed while the second at 675–700 nm is reinforced.

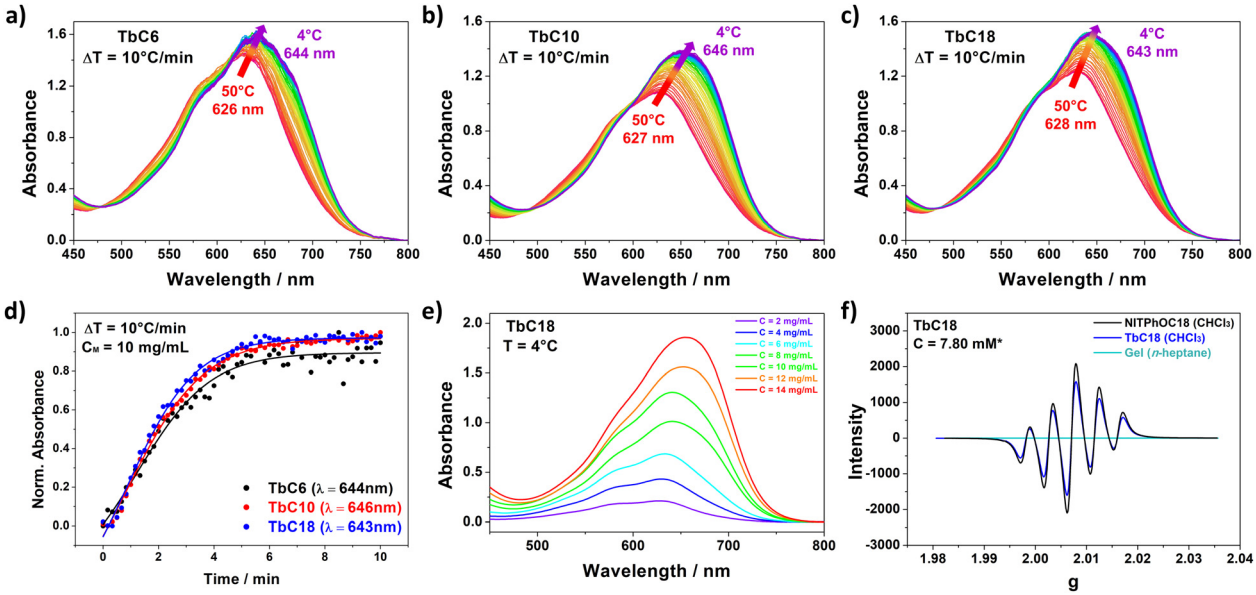

Fig. 2 (a)–(c) Variable temperature UV-visible spectrum of the *n*-heptane **TbCn** gels. (d) Time-resolved normalized absorbance of the *n*-heptane **TbCn** gels, (e) UV-visible spectrum at different mass concentration C_M of the *n*-heptane **TbC18** gel and (f) X-band EPR spectra of $CHCl_3$ solutions of **NITPhOC18** and **TbC18**, and *n*-heptane **TbC18** gel (*equivalent to C_M = 10 mg mL^{-1} of **TbC18** gel for comparison).

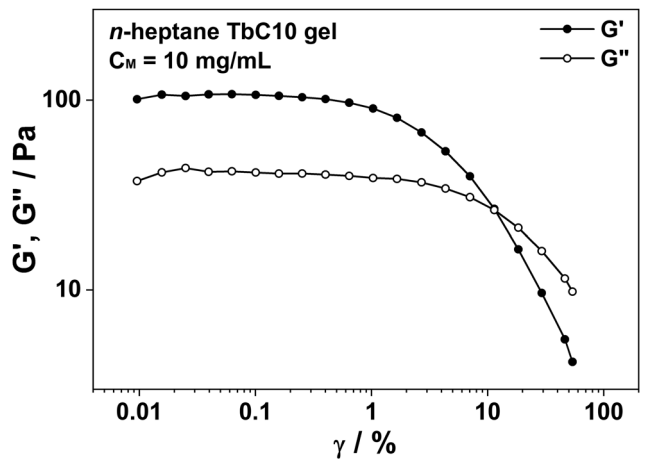

Fig. 3 Oscillatory strain dependence of shear storage (G') and loss (G'') modulus of **TbC10** gel (at 1 Hz frequency and T = 10 °C).

While the first shoulder could be associated with a lanthanide-radical coordination effect, the second is probably a consequence of the gelation. Indeed, it is easily reproduced on concentration-dependent measurements (Fig. 2e), and the shoulder appearance coincides with the formation of the gel phases at critical mass concentrations (C_M = 8 mg mL^{-1} for **TbC18** gel, see Fig. 1). By plotting the evolution of the normalized absorbance of this shoulder (Fig. S11, ESI†), we notice a bi-exponential growth. A putative hypothesis could be that the first growth is due to the formation of supramolecular nanotubes that trap solvent molecules and induce gelation. The second growth could be related to the bundling of nanotubes into bigger objects (see surface deposition). However clear evidence is lacking since temperature-independent measurement at 4 °C does not show any evolution because of the fast kinetics of the gel formation. Last, whatever the radical is, the time profiles associated with the growths are very much equivalent.

EPR spectroscopy measurements can be also used to monitor the sol–gel transition.[55–59] X-band EPR signals of **NITPhOCn** and uncoordinated **TbCn** solutions in $CHCl_3$ were recorded at room temperature and share the identical spectra with five lines of relative intensity 1 : 2 : 3 : 2 : 1 due to the hyperfine coupling between the two equivalent ^{14}N nuclei (Fig. S15 and S16, ESI†).[60] The *g*-factor and hyperfine coupling values are also in accordance with the literature, whatever the **NITPhOCn** derivative used (Table S3, ESI†).[61–63]

EPR spectra of both $CHCl_3$ solutions and *n*-heptane **TbCn** gels were recorded with identical experimental conditions to probe the influence of the gelation process on the mobility of the NIT molecules. As represented in Fig. 2f (and Fig. S12 and S13, ESI†), the signal of the free radicals is quenched upon gelation, with a signal intensity ratio of around 2000 : 2 between the uncoordinated **Pre-TbCn** powders in $CHCl_3$ solution and the gels of *n*-heptane. This indicates a strong electronic correlation of the radicals with the Tb^{III} ions, and also a substantial loss of mobility, likely due to the coordination of the latter with the $Tb(hfac)_3$ moieties that leads to the formation of a coordinated network.

From the above data, one can derive that the formation mechanism of these gels follows these different stages:

(i) At high temperature, the **NITPhOCn** radicals and the $Tb(hfac)_3$ complexes are uncoordinated in solution (characteristic blue colour and EPR signal of free **NITPhOCn**).

(ii) Upon rapid cooling down, these free species in solution start to coordinates progressively, resulting in the formation of

oligomers that grow in polymeric chains (redshift of the main UV-visible absorption band with isosbestic points and quenching of the free **NITPhOCn** EPR signal).

(iii) In the meantime, these polymeric chains self-assemble into wrapped supramolecular nanotubes that entrap solvent molecules to form gels.

Morphology of the metallogels

In our previous study, we were able to determine a molecular structural model of the **TbC18** gel through SAXS measurements from bulk gel and dried aligned fibres. It appeared that the gel was formed by supramolecular nanotubes consisting of eight helical chains wound together, whose porosity is filled with aliphatic solvent molecules (Fig. 4a).[41] Accordingly, the intensity profiles of **TbC6** and **TbC10** featured oscillations of similar periods (Fig. 4b) that can be fitted with eqn (1), related to the form factor of a hollow tube (with r_0 the radius of the tube, q the scattering vector and J_0 the Bessel function of zeroth order).

$$I(q) = \frac{J_0(qr_0)^2}{q^2} \quad (1)$$

Here, the best fits of the experimental data match for a radius r_0 = 1.77, 1.79, and 1.78 nm for the **TbC6**, **TbC10**, and **TbC18** gels resp., corresponding to nanotubes with diameters of $\varnothing_{gel} \approx$ 3.6 nm. Noteworthy, the minima of the X-ray scattering do not shift with the size of the alkyl chain beard by the NIT derivative used. This means that the diameter is conserved and that the formation of the supramolecular nanotubes is mainly dictated by the arrangement of the backbone chain, through π-stacking between the phenyl group of bridging NIT radicals and neighbouring aromatic $hfac^-$ planes.[64,65] It is therefore reasonable to assume that the supramolecular arrangement of entangled helical chains depicted previously for the **TbC18** gel can be extended to the shorter **TbC6** and **TbC10** derivatives.

Interestingly, time-dependent SAXS experiments have been also performed to evaluate the stability of each gel (Fig. 4b and c), and strengthen the observations made by optical microscopy (Fig. 4d). The intensity profiles of the aged **TbC6** and **TbC10** gels (after one day) show that the oscillations (related to the tubular gel state) disappear in benefit of sharp peaks due to demixion and crystallization processes within the amorphous gel matrix, while no changes are reported for the metastable **TbC18** gel, that can be stored for months at 4 °C with no sign of evolutions.

Magnetic properties

Static magnetic properties have been measured on frozen fresh *n*-heptane gels (C_M = 10 mg ml^{-1}) below the melting point of the solvent (T_M = 182 K). The temperature dependence of the product $\chi_M T$ shows a similar behaviour for the three **TbCn** gels (see Fig. S16, ESI†), with $\chi_M T_{(150K)}$ values of resp. 12.28, 12.13 and 12.25 emu K mol^{-1}. These values are close to the theoretical $\chi_M T$ of 12.19 emu K mol^{-1} for a free Tb^{III} ion (J = 6, g_J = 3/2) and an uncoupled radical (S = 1/2, g_S = 2) at 300 K. By

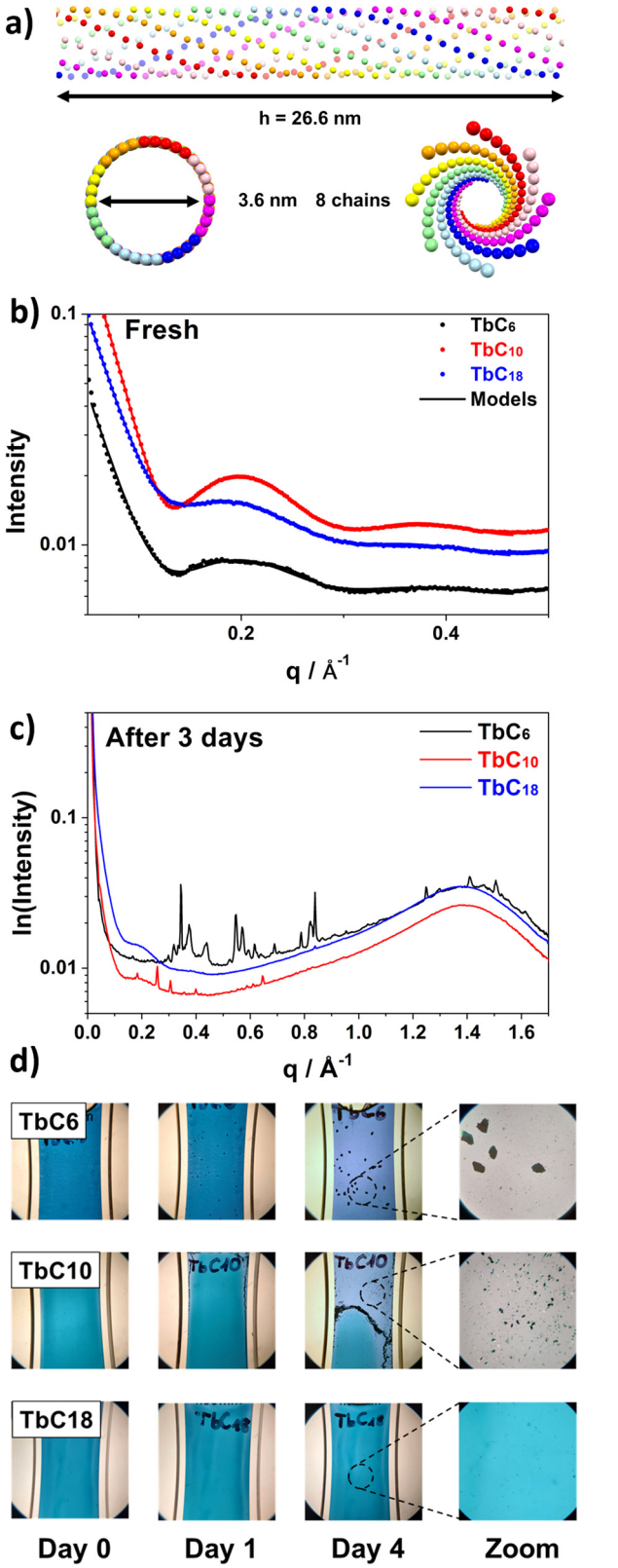

Fig. 4 (a) Representation of the supramolecular Tb^{III} nanotube of **TbC18** gel, reproduced from ref. 41 with permission from the Royal Society of Chemistry. (b) SAXS intensity profile spectra of fresh (with the best fits as plain lines). (c) and aged *n*-heptane TbCn gels. (d) Time-dependence evolution of the *n*-heptane **TbCn** gels at 4 °C under optical microscope (magnification *x*10 and *x*63, bottom).

Table 1 Characteristic values extracted from the temperature dependence of $\chi_M T$ and the Arrhenius plots of the *n*-heptane **TbCn** gels (C_M = 10 mg mL^{-1}) considering a double relaxation process

	TbC6		TbC10		TbC18	
C_{eff} (emu K mol^{-1})	11.77 ± 0.02		11.80 ± 0.03		11.90 ± 0.04	
$\Delta\xi_{(DC)}/k_B$ (K)	6.06 ± 0.04		4.96 ± 0.09		4.05 ± 0.05	
	Slow	Fast	Slow	Fast	Slow	Fast
Δ_{eff}/k_B (K)	43.0 ± 3.0	18.1 ± 0.7	35.2 ± 0.9	18.6 ± 0.5	45.2 ± 3.7	18.5 ± 0.4
τ_0 (s)	(3.1 ± 0.9) × 10^{-9}	(4.5 ± 1.4) × 10^{-7}	(4.7 ± 2.0) × 10^{-8}	(5.1 ± 1.2) × 10^{-7}	(5.3 ± 4.4) × 10^{-10}	(3.4 ± 0.7) × 10^{-7}
R^2	0.9555	0.9895	0.9958	0.9950	0.9741	0.9979

decreasing the temperature, these values stay constant then increase exponentially below 100 K to reach maxima of 23.66 emu K mol^{-1} at 5.5 K (**TbC6**), 22.76 and 21.73 emu K mol^{-1} at 4.5 K (for **TbC10** and **TbC18** resp.). A sharp decrease follows due to saturation effect, highlighted by AC measurements (Fig. S18, ESI†). The field dependence of the magnetization exhibits an abrupt rise starting at the lowest fields and quickly reaching saturation M_{sat} values of 5.1, 5.3 and 5.1 μ_B (for **TbC6**, **TbC10** and **TbC18** resp.), slightly below the theoretical value of 5.5 μ_B (Fig. S19, ESI†). Noteworthy, measurements conducted on the corresponding **Pre-TbCn** powders led to similar behaviours, depicted in Fig. S17–S20 (ESI†).

In agreement with the observation of molecular nanotube structure within all gels (Fig. 4b), these sharp increases of both the $\chi_M T$ product and the magnetization can be attributed to the onset of a magnetic correlation length along the chains, characteristic of SCM behaviour. The rise of a magnetic correlation along the SCMs by lowering the temperature can be then expressed as $\chi_M T = C_{eff}\exp(\Delta_\xi/k_B T)$, with C_{eff} a pre-exponential factor and Δ_ξ the correlation energy required to create a domain wall (Fig. S20, ESI†). These values, reported in Table 1 for the gels (and Table S4 for the precursors, ESI†), are close to the ones reported for the crystalline **TbC6** nanotubes (C_{eff} = 11.84 emu K mol^{-1} and $\Delta_{\xi(DC)}/k_B$ = 5.5 ± 0.5 K).[33]

The magnetic relaxation behaviour of the gels was then probed by dynamic (AC) susceptibility measurements with zero static external field. Clear temperature dependence of the in-phase ($\chi_{M'}$) and out-of-phase ($\chi_{M'}$) susceptibility signals are observed for each sample (Fig. S21–S24, ESI†), indicating the occurrence of slow relaxation of the magnetization for both **Pre-TbCn** and **TbCn gels**. In-phase and out-of-phase susceptibilities exhibit a noisy but unambiguous temperature dependence below 6 K, discarding the hypothesis of a ferro- or ferrimagnetic order as reported on similar Co-based systems,[66–68] and confirming the molecular origin of the relaxation of the magnetization. The out-of-phase susceptibility curves in Fig. S22 (ESI†) reveal the presence of two relaxing fractions for the gels below 3 K: a dominant one at higher frequencies (fast relaxation process) and a minor and broad contribution at lower frequencies (slow relaxation process). This additional contribution is stressed in the Argand diagrams, with the feature of a tail for the lower temperatures (Fig. S25, ESI†).

Characteristic relaxation times τ were deduced using a double relaxation Debye model and then fitted *via* an Arrhenius law $\tau = \tau_0\exp(\Delta\Delta_{eff}/k_B T)$ for both gels and precursors (Fig. S26, ESI†). The effective energy barrier Δ_{eff} and the pre-exponential factor τ_0 values extracted are listed in Table 1 below for the gels (and Table S5 for the precursors, ESI†).

All metrics extracted from the faster relaxation mode are similar for each gel and close to the ones reported for the **TbC6** crystal and the **TbC18** gel.[33,41] This is not surprising as all these compounds share a similar magnetic skeleton and a similar supramolecular organization. However, one can note the presence of two simultaneous relaxation processes is not common for SCM systems, although already reported in the literature.[68–70] Moreover, Ln-NIT systems are known to generate [Ln-NIT]$_n$ chains but also [NIT-Ln-NIT] complexes.[71,72] The latter can behave as SMM with U_{eff} and τ_0 values, which could be misinterpreted as Δ_{eff} and τ_0 resulting in an SCM relaxation.[73] Since we cannot discard the presence of traces of such molecules formed during the gelation we tested this hypothesis. The three [NIT-Tb-NIT] complexes based on **NITPhOC6**, **NITPhOC10** and **NITPhOC18** (Fig. S28 and Table S6, ESI†) have been synthesized and afford very similar molecular motive and CShM values (Table S7, ESI†). Once measured, these three samples show no χ''_M signal in zero external field, ruling out the possibility of spontaneous formation of these complexes upon gel and their contribution to the observed slow relaxation regime (Fig. S29, ESI†). A reasonable hypothesis is the simultaneous presence of short and long chains, both ruled by the finite-size regime.[69,74]

Magnetic hysteresis measurements were performed at 0.5 K. Both gels and precursor powders act as effective magnets with open hysteresis loops in our operating conditions (magnetic field sweep rate of 15.5 Oe s^{-1}, see Fig. 5 and Fig. S30, ESI†). In the case of the gels, the opening of the loop seems to follow a trend **TbC6** > **TbC10** > **TbC18** for the gels with the best performance attributed to the **TbC6** gel, with a coercive field of H_C = 3440 Oe and a remnant magnetization of M_R = 2.49 μ_B (Table S8, ESI†). This could be due to the difference in flexibility of the nanotubes formed, which averages out the overall magnetic anisotropy of the gel measured. This trend is nevertheless not observed for the precursor powders whose nearly stacked open hysteresis with the same pinched shapes testify of the preservation of the coordination organization that confers these magnetic properties after drying.

The transitions between the excited and ground magnetic states of *f*-elements are intrinsically dependent on the magnetic field[75] and can be observable through far-infrared magnetospectroscopy (FIRMS).[76] In our case, we measured infrared transmission spectra in all **Pre-TbCn** powder samples under applied magnetic fields up to 17.5T. The field-dependent part

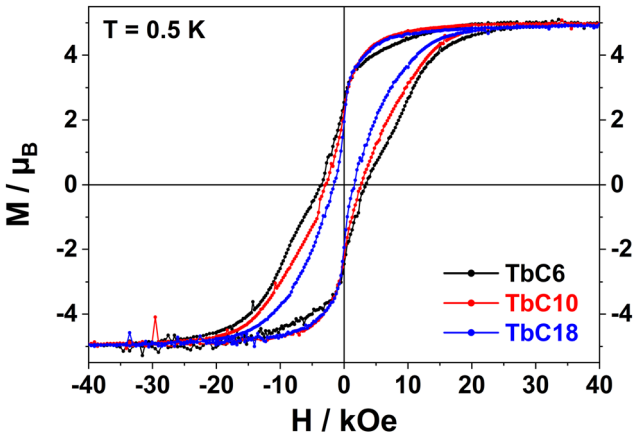

Fig. 5 Magnetic hysteresis curves of *n*-heptane **TbCn** gels (C_M = 10 mg mL^{-1}).

of infrared responses is only discernible within a limited spectral range, which is represented by the heatmap in Fig. 6.

However, the complexity of the pattern resulting from spin-phonon coupling and powder broadening,[77] hinders the precise determination of the crystal field transition energies. We attribute the spectroscopic features near 115, 131 and 155 cm^{-1} (Fig. 6 and Fig. S31, ESI†) to energy levels that closely resemble those reported by *ab initio* calculations for the first excited states of the crystalline **TbC6** nanotubes (38, 97, 120, 134 and 144 cm^{-1} respectively).[33] The distinct intensity of these features is related to the different concentrations of the magnetic molecules, whereas a similar pattern indicates identical crystal field levels in all precursors, and thereby the same nature of their magnetic properties.

Surface deposition

Finally, thin films of **TbCn** gels were prepared by spin-coating of drop-casted hot *n*-heptane solutions of **TbCn** on silicon wafer and characterized by AFM measurements to compare the morphology of the constituting fibres in Fig. 7.

Networks of entangled fibres are visible for each **TbCn** gel derivative, resulting from a self-assembly organization with

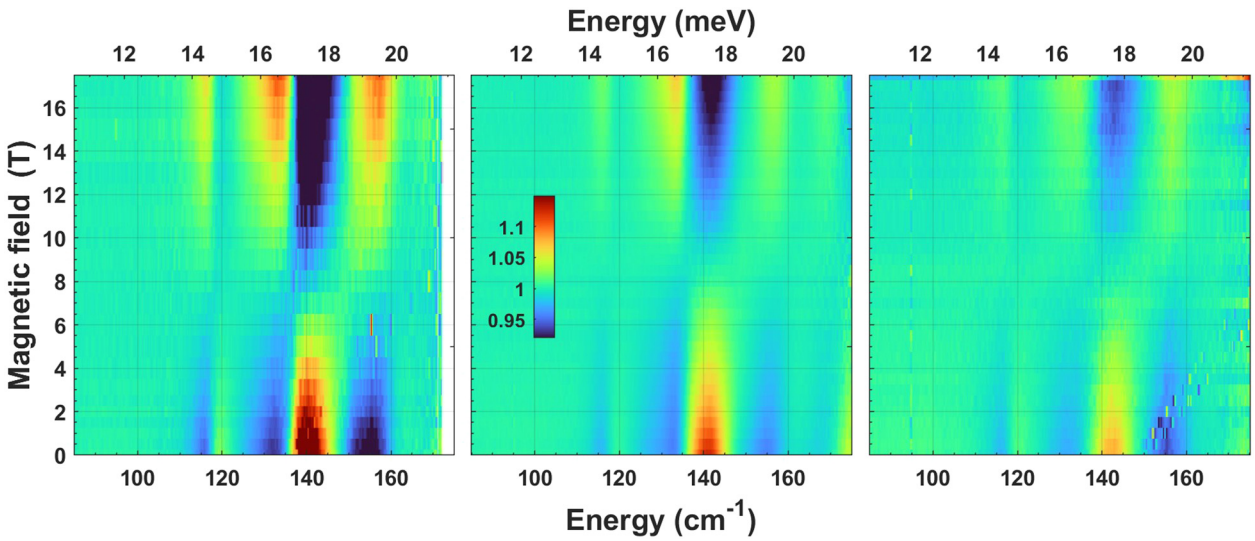

Fig. 6 FIRMS heatmaps measured for **Pre-TbC6** (left), **Pre-TbC10** (middle) and **Pre-TbC18** (right) at low temperature. The color scale represents the magnitude of relative changes in the IR transmission induced by magnetic fields. The experimental data were taken at 5.5 K and normalized to the average spectra as described in ESI† (Fig. S31, ESI†).

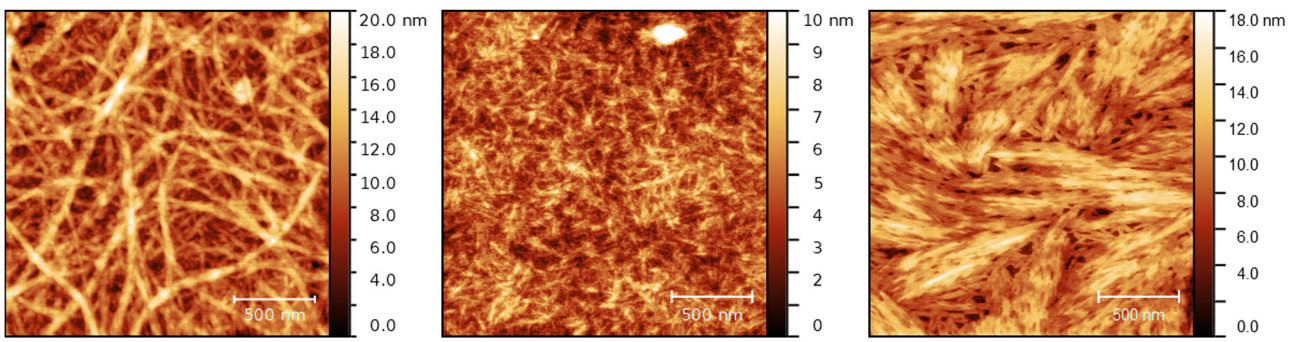

Fig. 7 AFM topography images of thick films of *n*-heptane **TbC6** (left), **TbC10** (middle) and **TbC18** (right) gels (C_M = 2 mg mL^{-1}).

noticeable differences. **TbC6** shows homogeneous and well-defined tubular structures, long of several hundreds of nanometers to few micrometers. A rough estimation of tens of nanometres of diameter, in line with the values deducted by SAXS experiments for one tube, indicates that such fibres are made of wrapping of several tubular units. Similar conclusions hold for the thin film of **TbC10** gel, although the fibres appear smaller and randomly distributed. Finally, for the **TbC18** thin film, the fibres seem organized in dense brush-like bundles of small fibres.

Overall, these AFM images show the strong influence of the aliphatic chain length from the NIT radical on the resulting morphologies observed on surface, despite the chemical and structural similarities deducted from the previous SAXS study. In particular, the longer is the alkyl chain, the denser results the network of fibres observed by AFM. Accordingly, the nominal diameter of the fibres appears smaller and provides a more regular arrangement of piled fibres when the **TbC18** system is considered. This evidence suggests a promising strategy to promote a long-range ordering of these fibres, thus approaching the realisation of regular arrays of SCMs.

Conclusion

In this study, we investigated the best conditions to obtain stable deposits of supramolecular nanotubes in gel media (metallogels). Since these nanotubes are made of woven chains constructed by the alternance of Tb and nitronyl-nitroxide radical building blocks, we evaluate the influence of the size of the alkyl chain grafted on the radical (**NITPhOCn**, with $n = 6$, 10, or 18) on the synthesis, stability, physico-chemical properties of metallogels as well as their ability to form deposits on surface.

We demonstrated by temperature-dependent UV-Vis studies that whatever the length of alkyl chain is, gelation kinetics are comparable. On the contrary, we observed striking differences from the thermodynamic point of view as liquid-gel pseudo-phase diagrams show that the longer the alkyl chain, the smaller the gel domain. As expected, gel stability against crystallization is clearly improved for longer alkyl chains.

Importantly, SAXS measurements showed that all three gels share a similar supramolecular organization and are all made of eight woven helical chains forming nanotubes with a diameter of 3.6 nm.

Similarly, FIRMS measurements demonstrate that the molecular magnetic backbone and the electronic feature of the magnetic Tb^{III} ions are not sensitive to alkyl chain variation. This induces a similar Single-Chain Magnet behaviour in gel media with clear magnetic hysteresis loops for all samples.

Last, surface deposition is largely facilitated for gels bearing long alkyl chains (**TbC18**) that form thick films of molecular nanotubes. In these films, the nanotubes are arranged more regularly compared with the disordered organization observed with shorter chains (**TbC6**, **TbC10**). This suggests a key role of these alkyl chains also in the lateral long-range arrangement of nanotubes in ordered bunches. This last observation paves the way toward the exploration of regular arrays of SCM, a mandatory step for individual magnetic addressing of these objects.

This study demonstrates that in metallogels of supramolecular nanotubes, increasing alkyl chain length induces more delicate gelation conditions but provides gels with improved stability against crystallization and enhanced deposition ability. These modifications do not damage the electronic and magnetic properties of the chains and most of all their SCM behaviour. These findings are of interest for the design of supramolecular structures on surfaces using gel intermediates.

Author contributions

F. Houard: conceptualization, resources, data curation, investigation, visualization, writing – original draft, writing – review & editing. A. Olivier: investigation. G. Cucinotta: investigation. O. Galangau: conceptualization, investigation, writing – review & editing. M. Gautier: investigation. F. Camerel: investigation. T. Guizouarn: investigation. T. Roisnel: investigation. B. Le Guennic: writing – review & editing. M. Ozerov: investigation, writing – review & editing. Y. Suffren: investigation. G. Calvez: writing – review & editing. C. Daiguebonne: writing – review & editing. O. Guillou: writing – review & editing. F. Artzner: software, formal analysis, investigation, writing – review & editing. M. Mannini: conceptualization, supervision, funding acquisition, writing – review & editing. K. Bernot: conceptualization, writing – original draft, writing – review & editing, supervision, funding acquisition and project administration.

Conflicts of interest

There are no conflicts to declare.

Acknowledgements

We acknowledged the French Ministry of High Education and Research (MESRI), Region Bretagne, Rennes Metropole, INSA PPI program, and CNRS *via* FloRennes PICS Program. K. B. acknowledges Institut Universitaire de France. F. H. acknowledges SATT Ouest Valorisation for funding. M. M. and G. C. acknowledge the Italian MIUR, through the Project ''Dipartimenti di Eccellenza'' 2018–2022 (ref. no. B96C1700020008) and Fondazione Cassa di Risparmio di Firenze (Project SPINE-2 2020.1634) for the financial support. Surface depositions have been carried out at the surface science laboratories of the MatchLab Interdepartmental Research Unit, University of Florence. Part of the work was performed at the National High Magnetic Field Laboratory, which is supported by the National Science Foundation Cooperative Agreement No. DMR-2128556 and the State of Florida.

Notes and references

1 O. Gutfleisch, M. A. Willard, E. Brück, C. H. Chen, S. G. Sankar and J. P. Liu, *Adv. Mater.*, 2011, **23**, 821–842.
2 D. A. Thompson and J. S. Best, *IBM J. Res. Dev.*, 2000, **44**, 311–322.
3 D. Reinsel, J. Gantz and J. Rydning, *The Digitization of the World from Edge to Core*, IDC, USA, 2018.
4 C. Benelli and D. Gatteschi, *Introduction to molecular magnetism: from transition metals to lanthanides*, Wiley-VCH, Weinheim, 2015.
5 *Molecular magnetic materials: concepts and applications*, ed., B. Sieklucka and D. Pinkowicz, Wiley-VCH Verlag GmbH & Co. KGaA, Weinheim, 2017.
6 C. A. P. Goodwin, *Dalton Trans.*, 2020, **49**, 14320–14337.
7 K. Bernot, *Eur. J. Inorg. Chem.*, 2023, e202300336.
8 F. Neese and D. A. Pantazis, *Faraday Discuss.*, 2011, **148**, 229–238.
9 J. D. Rinehart and J. R. Long, *Chem. Sci.*, 2011, **2**, 2078.
10 Z. Zhu and J. Tang, in *Organometallic Magnets*, ed. V. Chandrasekhar and F. Pointillart, Springer International Publishing, Cham, 2018, vol. 64, pp. 191–226.
11 N. Ishikawa, M. Sugita, T. Ishikawa, S. Koshihara and Y. Kaizu, *J. Am. Chem. Soc.*, 2003, **125**, 8694–8695.
12 B. M. Day, F.-S. Guo and R. A. Layfield, *Acc. Chem. Res.*, 2018, **51**, 1880–1889.
13 D. Gatteschi, A. Cornia, M. Mannini and R. Sessoli, *Inorg. Chem.*, 2009, **48**, 3408–3419.
14 A. Cornia and M. Mannini, in *Molecular Nanomagnets and Related Phenomena*, ed. S. Gao, Springer Berlin Heidelberg, Berlin, Heidelberg, 2014, vol. 164, pp. 293–330.
15 G. Gabarró-Riera, G. Aromí and E. C. Sañudo, *Coord. Chem. Rev.*, 2023, **475**, 214858.
16 D. Gatteschi and R. Sessoli, *Angew. Chem., Int. Ed.*, 2003, **42**, 268–297.
17 M. N. Leuenberger and D. Loss, *Nature*, 2001, **410**, 789–793.
18 S. Jiang, K. Goß, C. Cervetti and L. Bogani, *Sci. China: Chem.*, 2012, **55**, 867–882.
19 L. Bogani, in *Molecular Nanomagnets and Related Phenomena*, ed. S. Gao, Springer Berlin Heidelberg, Berlin, Heidelberg, 2014, vol. 164, pp. 331–381.
20 E. Coronado, *Nat. Rev. Mater.*, 2019, **5**, 87–104.
21 A. J. Heinrich, W. D. Oliver, L. M. K. Vandersypen, A. Ardavan, R. Sessoli, D. Loss, A. B. Jayich, J. Fernandez-Rossier, A. Laucht and A. Morello, *Nat. Nanotechnol.*, 2021, **16**, 1318–1329.
22 L. Bogani, A. Vindigni, R. Sessoli and D. Gatteschi, *J. Mater. Chem.*, 2008, **18**, 4750–4758.
23 W.-X. Zhang, R. Ishikawa, B. Breedlove and M. Yamashita, *RSC Adv.*, 2013, **3**, 3772.
24 K. S. Pedersen, A. Vindigni, R. Sessoli, C. Coulon and R. Clérac, in *Molecular Magnetic Materials*, ed. B. Sieklucka and D. Pinkowicz, Wiley-VCH Verlag GmbH & Co. KGaA, Weinheim, Germany, 2016, pp. 131–159.
25 R. J. Glauber, *J. Math. Phys.*, 1963, **4**, 294–307.
26 R. Sessoli, *Angew. Chem., Int. Ed.*, 2008, **47**, 5508–5510.
27 L. B. Volodarsky, V. A. Reznikov and V. I. Ovcharenko, *Synthetic chemistry of stable nitroxides*, CRC Press, Boca Raton, FL, 2018.
28 A. Caneschi, D. Gatteschi, R. Sessoli and P. Rey, *Acc. Chem. Res.*, 1989, **22**, 392–398.
29 C. Benelli, A. Caneschi, D. Gatteschi, L. Pardi and P. Rey, *Inorg. Chem.*, 1990, **29**, 4223–4228.
30 E. V. Tretyakov and V. I. Ovcharenko, *Russ. Chem. Rev.*, 2009, **78**, 971–1012.
31 X. Meng, W. Shi and P. Cheng, *Coord. Chem. Rev.*, 2019, **378**, 134–150.
32 D. Luneau, *Eur. J. Inorg. Chem.*, 2020, 597–604.
33 F. Houard, Q. Evrard, G. Calvez, Y. Suffren, C. Daiguebonne, O. Guillou, F. Gendron, B. Le Guennic, T. Guizouarn, V. Dorcet, M. Mannini and K. Bernot, *Angew. Chem., Int. Ed.*, 2020, **59**, 780–784.
34 P. R. A. Chivers and D. K. Smith, *Nat. Rev. Mater.*, 2019, **4**, 463–478.
35 J. Zhang and C.-Y. Su, *Coord. Chem. Rev.*, 2013, **257**, 1373–1408.
36 H. Wu, J. Zheng, A. Kjøniksen, W. Wang, Y. Zhang and J. Ma, *Adv. Mater.*, 2019, **31**, 1806204.
37 P. Sutar and T. K. Maji, *Dalton Trans.*, 2020, **49**, 7658–7672.
38 G. Picci, C. Caltagirone, A. Garau, V. Lippolis, J. Milia and J. W. Steed, *Coord. Chem. Rev.*, 2023, **492**, 215225.
39 O. Roubeau, A. Colin, V. Schmitt and R. Clérac, *Angew. Chem., Int. Ed.*, 2004, **43**, 3283–3286.
40 T. Fujigaya, D.-L. Jiang and T. Aida, *Chem. – Asian J.*, 2007, **2**, 106–113.
41 F. Houard, G. Cucinotta, T. Guizouarn, Y. Suffren, G. Calvez, C. Daiguebonne, O. Guillou, F. Artzner, M. Mannini and K. Bernot, *Mater. Horiz.*, 2023, **10**, 547–555.
42 L. Zhang, X. Wang, T. Wang and M. Liu, *Small*, 2015, **11**, 1025–1038.
43 J. Cui, Y. Zheng, Z. Shen and X. Wan, *Langmuir*, 2010, **26**, 15508–15515.
44 A. Sandeep, V. K. Praveen, D. S. Shankar Rao, S. Krishna Prasad and A. Ajayaghosh, *ACS Omega*, 2018, **3**, 4392–4399.
45 A. Pal and J. Dey, *Soft Matter*, 2011, **7**, 10369.
46 S. K. Samanta and S. Bhattacharya, *J. Mater. Chem.*, 2012, **22**, 25277.
47 C. Po, A. Y.-Y. Tam and V. W.-W. Yam, *Chem. Sci.*, 2014, **5**, 2688.
48 E. F. Ullman, J. H. Osiecki, D. G. B. Boocock and R. Darcy, *J. Am. Chem. Soc.*, 1972, **94**, 7049–7059.
49 Q. Evrard, F. Houard, C. Daiguebonne, G. Calvez, Y. Suffren, O. Guillou, M. Mannini and K. Bernot, *Inorg. Chem.*, 2020, **59**, 9215–9226.
50 A. Caneschi, D. Gatteschi, J. Laugier, P. Rey, R. Sessoli and C. Zanchini, *J. Am. Chem. Soc.*, 1988, **110**, 2795–2799.
51 A. Caneschi, D. Gatteschi, N. Lalioti, C. Sangregorio and R. Sessoli, *J. Chem. Soc., Dalton Trans.*, 2000, 3907–3912.
52 L. Bogani, C. Sangregorio, R. Sessoli and D. Gatteschi, *Angew. Chem., Int. Ed.*, 2005, **44**, 5817–5821.
53 G. Bussière, R. Beaulac, H. Bélisle, C. Lescop, D. Luneau, P. Rey and C. Reber, *Transition Metal and Rare Earth*

Compounds, Springer Berlin Heidelberg, Berlin, Heidelberg, 2004, vol. 241, pp. 97–118.
54 C. Lescop, E. Belorizky, D. Luneau and P. Rey, *Inorg. Chem.*, 2002, **41**, 3375–3384.
55 P. Terech, R. Ramasseul and F. Volino, *J. Colloid Interface Sci.*, 1983, **91**, 280–282.
56 P. Terech, *J. Colloid Interface Sci.*, 1985, **107**, 244–255.
57 M. Kveder, M. Andreis, J. Makarević, M. Jokić and B. Rakvin, *Chem. Phys. Lett.*, 2006, **420**, 443–447.
58 M. Mannini, S. Cicchi, D. Berti, A. Caneschi, A. Brandi, L. Lascialfari and L. Sorace, *ChemPlusChem*, 2013, **78**, 149–156.
59 Y. Takemoto, T. Yamamoto, N. Ikuma, Y. Uchida, K. Suzuki, S. Shimono, H. Takahashi, N. Sato, Y. Oba, R. Inoue, M. Sugiyama, H. Tsue, T. Kato, J. Yamauchi and R. Tamura, *Soft Matter*, 2015, **11**, 5563–5570.
60 N. Hogg, *Free Radical Biol. Med.*, 2010, **49**, 122–129.
61 A. Collauto, M. Mannini, L. Sorace, A. Barbon, M. Brustolon and D. Gatteschi, *J. Mater. Chem.*, 2012, **22**, 22272.
62 R. Kakavandi, S.-A. Savu, L. Sorace, D. Rovai, M. Mannini and M. B. Casu, *J. Phys. Chem. C*, 2014, **118**, 8044–8049.
63 L. Poggini, G. Cucinotta, L. Sorace, A. Caneschi, D. Gatteschi, R. Sessoli and M. Mannini, *Rend. Fis. Acc. Lincei*, 2018, **29**, 623–630.
64 C. Janiak, *J. Chem. Soc., Dalton Trans.*, 2000, 3885–3896.
65 K. S. Kim, S. Karthikeyan and N. J. Singh, *J. Chem. Theory Comput.*, 2011, **7**, 3471–3477.
66 N. Ishii, Y. Okamura, S. Chiba, T. Nogami and T. Ishida, *J. Am. Chem. Soc.*, 2008, **130**, 24–25.
67 Y. Okamura, N. Ishii, T. Nogami and T. Ishida, *Bull. Chem. Soc. Jpn.*, 2010, **83**, 716–725.
68 X. Liu, X. Feng, K. R. Meihaus, X. Meng, Y. Zhang, L. Li, J. Liu, K. S. Pedersen, L. Keller, W. Shi, Y. Zhang, P. Cheng and J. R. Long, *Angew. Chem., Int. Ed.*, 2020, **59**, 10610–10618.
69 M. G. F. Vaz, R. A. A. Cassaro, H. Akpinar, J. A. Schlueter, P. M. Lahti and M. A. Novak, *Chem. – Eur. J.*, 2014, **20**, 5460–5467.
70 X. Huang, K. Wang, J. Han, J. Xie, L. Li and J.-P. Sutter, *Dalton Trans.*, 2021, **50**, 11992–11998.
71 K. Bernot, F. Pointillart, P. Rosa, M. Etienne, R. Sessoli and D. Gatteschi, *Chem. Commun.*, 2010, **46**, 6458.
72 J. Jung, M. Puget, O. Cador, K. Bernot, C. J. Calzado and B. Le Guennic, *Inorg. Chem.*, 2017, **56**, 6788–6801.
73 K. Bernot, J. Luzon, L. Bogani, M. Etienne, C. Sangregorio, M. Shanmugam, A. Caneschi, R. Sessoli and D. Gatteschi, *J. Am. Chem. Soc.*, 2009, **131**, 5573–5579.
74 L. Bogani, R. Sessoli, M. G. Pini, A. Rettori, M. A. Novak, P. Rosa, M. Massi, M. E. Fedi, L. Giuntini, A. Caneschi and D. Gatteschi, *Phys. Rev. B: Condens. Matter Mater. Phys.*, 2005, **72**, 064406.
75 D. J. Newman, *Adv. Phys.*, 1971, **20**, 197–256.
76 M. Ozerov, N. Anand, L. J. Van De Burgt, Z. Lu, J. Holleman, H. Zhou, S. McGill and C. Beekman, *Phys. Rev. B*, 2022, **105**, 165102.
77 J. G. C. Kragskow, J. Marbey, C. D. Buch, J. Nehrkorn, M. Ozerov, S. Piligkos, S. Hill and N. F. Chilton, *Nat. Commun.*, 2022, **13**, 825.